JOURNAL OF MATERIALS SCIENCE 30 (1995) 2541–2548

Dynamic mechanical response of an SiC_p/Al–Li (8090) composite

R. U. VAIDYA, A. K. ZUREK
Materials Science and Technology, Los Alamos National Laboratory, Los Alamos, NM 87545, USA

The dynamic mechanical response of an Al–Li alloy (8090) and SiC particle-reinforced 8090 composite was studied. The strain-hardening behaviour of the alloy was found to change significantly with increasing strain rate. Increasing the strain rate from 10^{-3} s^{-1} to 6500 s^{-1} doubled the strain-hardening coefficient of the alloy. The presence of the particles in the matrix did not affect the strain-hardening coefficient of the alloy. This was attributed to the relatively weak bonding between the particles and the matrix. An orientation effect was observed in the composite samples as a result of the preferential orientation of the reinforcing particles during the extrusion process. The thermal expansion behaviour of the composite samples was found to agree well with Kerner's model, and provided further evidence of the weak interfacial bonding.

1. Introduction

Aluminium matrices reinforced with ceramic particles have been studied for many years. These discontinuous composites have a number of practical advantages over continuous fibre-reinforced composites, the two most important ones being ease of fabrication, and isotropy. In recent years, aluminium–lithium alloys have been at the forefront of active research. It has been shown [1, 2] that small additions of lithium to aluminium can increase the stiffness, and at the same time reduce the density of the parent metal aluminium. These alloys are being considered for aerospace applications.

Additions of ceramic particles such as SiC can enhance the strength and stiffness of aluminium–lithium alloys even further, Table I [1]. Addition of 15 vol % SiC particles to an Al–Li alloy can enhance the stiffness of the alloy by as much as 25%. Additionally, SiC has been shown to improve other important properties such as wear resistance [3], creep resistance [4], and high-temperature strength [5] of other aluminium alloys. Enhancement in these properties must also be accounted for if such aluminium–lithium alloys are to be considered in aerospace applications.

The static mechanical properties of aluminium alloys and composites have been documented. However, one aspect of the mechanical behaviour which has been relatively ignored is the effect of strain rate on the response of such materials. When used in structural applications, these materials can be intentionally or inadvertently subjected to high strain rates. How these materials behave under such conditions can dictate the potential uses, and also provide an understanding of what response to expect from them.

The mechanical properties of continuous aligned-fibre composites have been reasonably well predicted from fibre-strengthening theories in which the properties are largely determined by the volume fraction and strength of the reinforcement phase, matrix and interface. However, the case of discontinuous composites is more complicated. The distribution of the reinforcements can change significantly with fabrication, and subsequently affect the mechanical properties.

In this work, we investigated the dynamic mechanical response of an aluminium–lithium alloy and an SiC_p-reinforced aluminium–lithium alloy. The observed behaviour has been correlated with the distribution of the particles in the matrix.

2. Experimental procedure

The nominal composition of the alloy (8090) used in the present study is provided in Table II. Both unreinforced and reinforced alloys containing 15 vol % SiC particles (SiC_p) were studied. The samples were produced by a spray-casting technique (Osprey). The materials were obtained in the form of extruded billets, 45 cm in length and 7.5 cm wide. The thickness of the billet was 1.25 cm. The extrusion process was carried out in one step at 538 °C, for 34 s, with an extrusion ratio of 17.1 : 1. The continuous extrusion pressure was 4.1 MPa.

Cylindrical test specimens (0.5 cm × 0.5 cm) were machined out of the extruded stock materials (unreinforced alloy and composite), in three different directions as shown in Fig. 1. All of the samples were heated in air at 450 °C for 8 h, and furnace cooled to room temperature. The temperature and time were selected based on earlier studies carried out on the material [6].

The static and dynamic mechanical responses of the unreinforced alloy and composite samples were measured in compression using a conventional screw-driven testing machine, and a Split Hopkinson

0022–2461

TABLE I Advantages of Al–Li alloy and its composites over conventional aluminium alloys and composites [1]

Material	Modulus (GPa)	Density ($g cm^{-3}$)	Specific modulus (GPA/unit density)
Al 2024 alloy	72	2.8	25.7
Al–Li 8090 alloy	80	2.55	31.5
Al 2024 alloy + 15 vol % SiC_p	95	2.84	33.5
Al–Li 8090 alloy + 15 vol % SiC_p	100	2.62	38.2

TABLE II Nominal composition of Al–Li 8090 alloy

	Li	Cu	Mg	Zr	Fe	Si	Al
Composition (wt %)	2.2	1.1	0.5	0.12	0.08	0.04	Balance

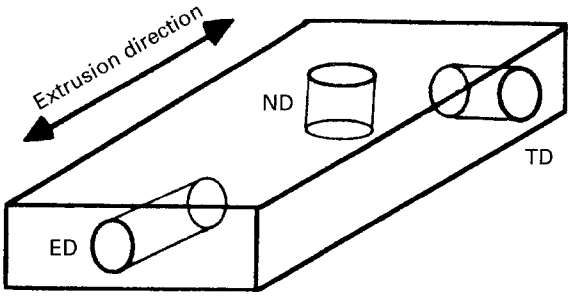

Figure 1 Schematic illustration of the various specimen orientations.

Pressure Bar. All of the tests were performed at room temperature. The static tests were done at a strain rate of $10^{-3} s^{-1}$, while the dynamic tests were carried out at strain rates of 2500 and 6500 s^{-1}.

Thermal expansion measurements were made with an Orton dilatometer (1000 D) according to ASTM Standard C-372/81. The dilatometer was interfaced with a computer which was used to calculate and record the experimental data. A sample length of 2.54 + 0.3 cm was used in all of the tests. The thermal expansion of the samples was detected by a linear variable differential transformer having a resolution of 0.25%, in the range of 0.318 cm, with an error range of 65×10^{-4} cm.

Almost all of the thermal expansion measurements on the unreinforced alloy and composite samples were done in the temperature interval 20–500 °C. This temperature range was selected so as to include the entire usable range of the materials, without inducing any liquid-phase formation in the alloy. The thermal expansion of the unreinforced alloy and composite samples was recorded at a heating/cooling rate of 5 °C min^{-1}.

Optical, scanning, and transmission electron microscopy was carried out to characterize the microstructure.

3. Results and discussion

Results of the quasistatic and dynamic mechanical tests for the unreinforced alloy and composite material have been compared in three different directions, and at three different strain rates in Figs 2 and 3. From the data for the unreinforced alloy, Fig. 2, it is evident that the strain rate has a significant effect on not only the overall strength but also on the strain hardening. For a strain rate of $10^{-3} s^{-1}$ the strain hardening (increase in the stress in a given strain range) measured in the strain range 0.15–0.25, was 300 MPa per unit strain. The strain hardening more than doubled to 700 MPa per unit strain, in the same strain range, but at a strain rate of 6500 s^{-1}. The mechanical response, however, did not change much between the strain rates of 2500 and 6500 s^{-1}. Orientation of the test axis with respect to the sample extrusion direction has a minimal effect on the mechanical response of the unreinforced material.

The composite, on the other hand, exhibits a measurable difference in the strength in the three tested directions, at all strain rates (Fig. 3). The strength in the extruded direction (ED) is higher compared to the strength in the transverse direction (TD), which in turn is higher than the strength in the normal direction (ND). The yield stress for the composite samples is also expectedly larger than for the unreinforced alloy (all strain rates and directions). The measured strain hardening of the composite samples is very similar to those of the unreinforced alloy samples tested at the same strain rates, as is the low strain-rate sensitivity between strain rates of 2500 and 6500 s^{-1}. These data indicate that the reinforcing particles did not contribute to the strain hardening of the matrix, and the observed strain-rate sensitivity between 10^{-3} and 6500 s^{-1} was primarily a result of the alloy behaviour.

An equation describing the dependence of the hardening rate in a metal as a function of strain rate is [7]

$$\theta = \theta_h - \theta_r \quad (1)$$

where θ is the total hardening rate, θ_h is the hardening component due to dislocation generation and storage, and θ_r is the softening component due to dynamic recovery through dislocation rearrangement. Both of these quantities are functions of the stress, σ, strain rate, ε, and temperature, T.

For a metal matrix composite, the equation is modified as [8]

$$\theta = \eta(\theta_h - \theta_r - \theta_{ad}) \quad (2)$$

where θ_{ad} is the accumulative damage term due to interface damage or particle cracking and η is the ratio of the strength of the composite at two different temperatures or strain rates for the same microstructure. Inclusion of η is important because the ratio of the flow stresses at two different temperatures or strain rates is constant irrespective of the total strain if Cottrell–Stokes law is obeyed.

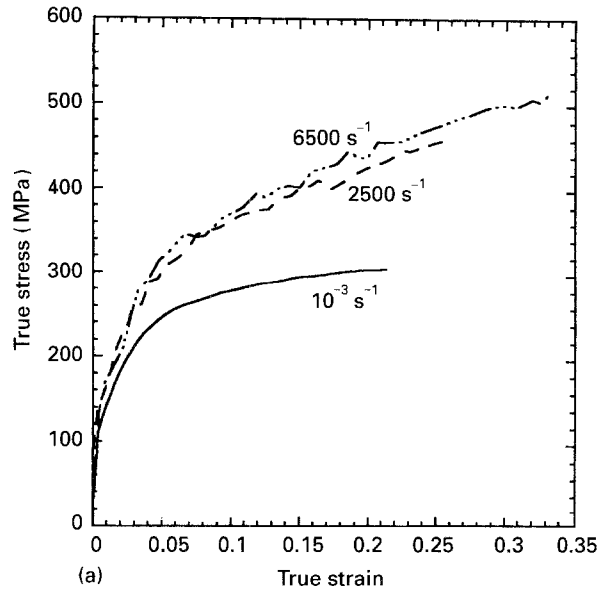

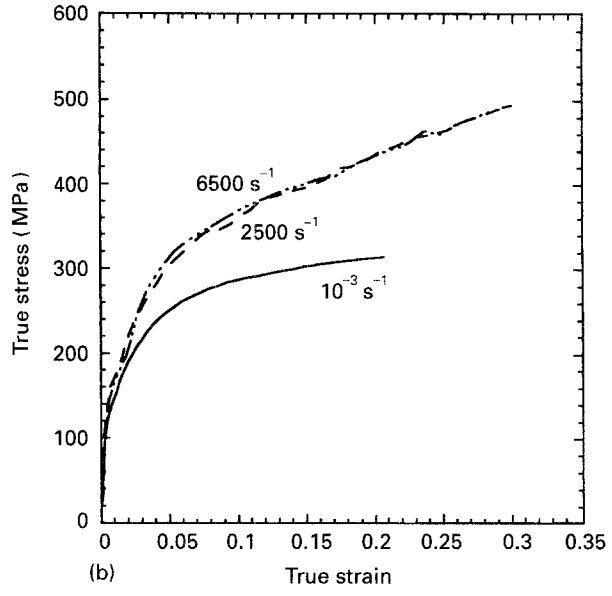

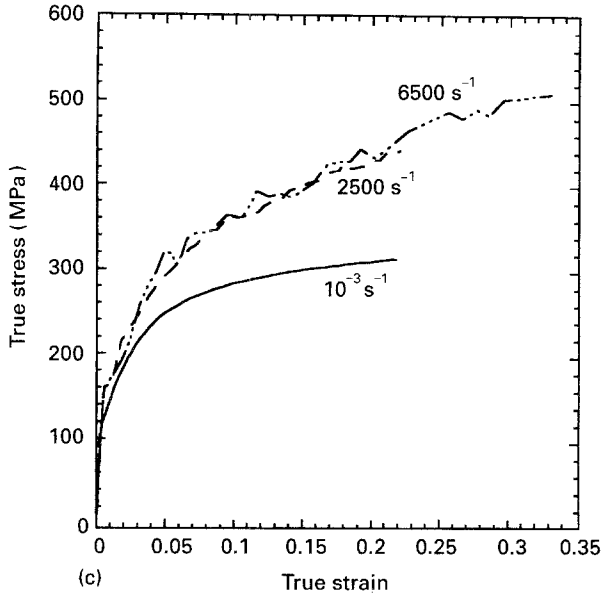

Figure 2 Stress–strain response for the unreinforced alloy at different strain rates. (a) ED direction, (b) TD direction, (c) ND direction.

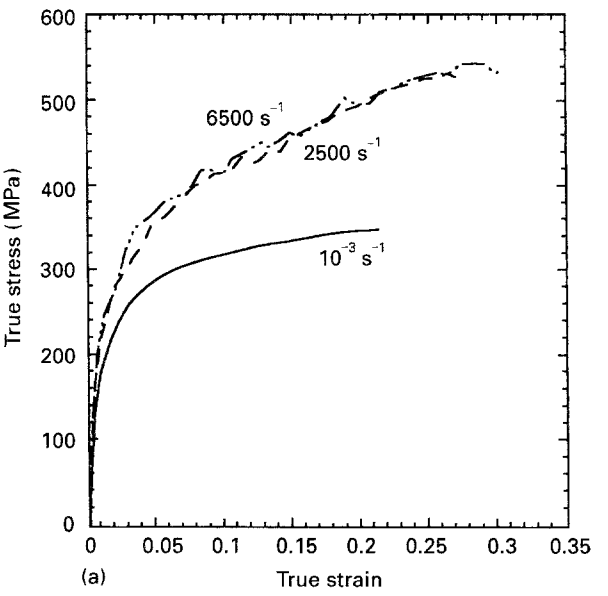

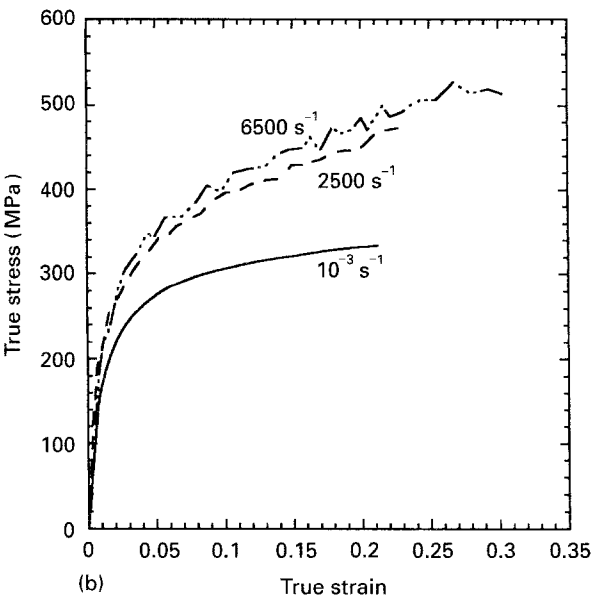

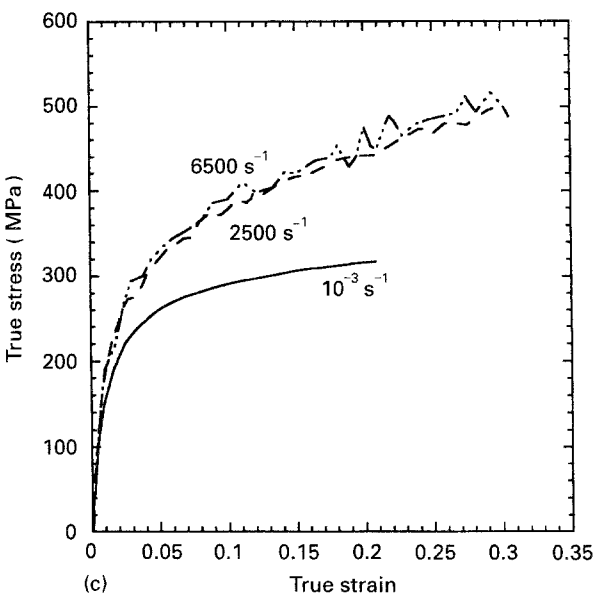

Figure 3 Stress–strain response for the composite samples at different strain rates. (a) ED direction, (b) TD direction, (c) ND direction.

We believe that η is dependent on four factors:

1. bonding between the particles and matrix;
2. the difference in the coefficient of thermal expansion between the particles and matrix, which can induce dislocations at the interface;
3. the size of the reinforcements;
4. distribution and orientation of the reinforcements.

Enhanced bonding, and a larger difference in the thermal expansion coefficient (between the matrix and reinforcement) lead to an increase in η. Increase in the size of the reinforcements decreases η. Optical and scanning microscopy revealed very little particle damage in the composite samples in all orientations, prior to testing. With the large difference in the coefficient of thermal expansion between the matrix ($21.2 \times 10^{-6}\,°C^{-1}$) and the SiC particles ($4.5 \times 10^{-6}\,°C^{-1}$), one would expect a significant enhancement in the strain hardening because of the large dislocation density induced in the matrix in close vicinity to the particles, as a result of the large thermal expansion mismatch between the reinforcing particles and matrix. However, the strain hardening in the composite is not enhanced over the unreinforced alloy.

A scanning electron micrograph of a composite sample fractured in tension can be seen in Fig. 4. The micrograph revealed the presence of particle cracking and particle/matrix debonding in the fracture surface. However, no particle/matrix debonding was observed in composite samples tested in compression (albeit not to failure). A possible explanation of the discrepancy in the observations is as follows: during the fabrication process, the alloy and the reinforcing particles are cooled down from elevated temperatures. Large thermal stresses are generated in the vicinity of the particle/matrix interface because of the three-dimensional constraint imposed on the particles by the rapidly shrinking matrix. However, on axial loading to failure (in tension), the interfacial constraint is relaxed in the direction of the applied stress, and the interface debonds. It should be possible to observe interfacial debonding in the samples tested in compression, provided the samples are subjected to a larger strain than that administered in the present tests.

Dislocations produced in the matrix, either as a result of thermal expansion mismatch or mechanical deformation, can escape at the debonded (free surface) and cracked interfaces. In addition, the constraint exerted by the reinforcing particles on the plastic deformation of the matrix is reduced as a result of weak particle/matrix bonding.

Transmission electron microscopy was carried out to determine the possible causes of the weak interface. A micrograph of the particle/matrix interface, in the as-received and annealed material, can be seen in Fig. 5. No reaction products were observed at the interface. However, this does not necessarily mean that a strong bonding between the particles and matrix exists. The wetting characteristics of the particles by the alloy could be the contributing factors to the weak bonding, especially because the alloy also contains lithium. Furthermore, we found that the dislocation density in the matrix, even in samples deformed at high strain rates, was very small compared

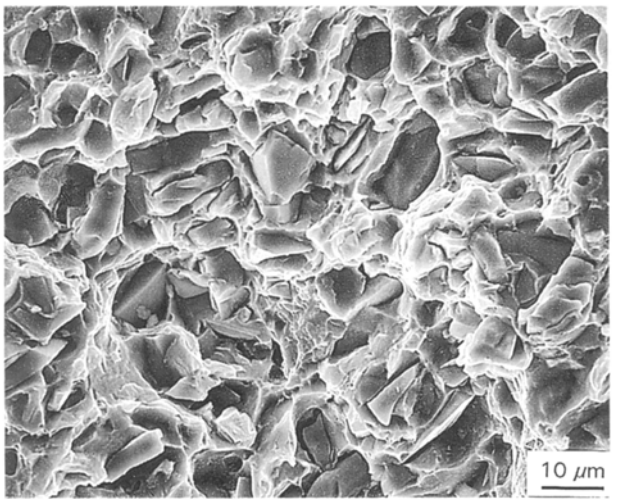

Figure 4 Scanning electron micrograph of the fractured surface of a composite sample illustrating extensive particle/matrix debonding.

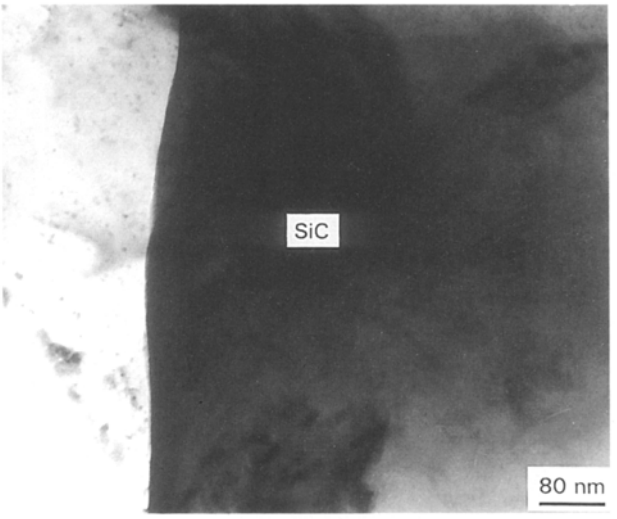

Figure 5 Transmission electron micrograph of a particle/matrix interface in the as-received and annealed states.

to the dislocation densities in other ceramic particle-reinforced aluminium matrix composites. We have also shown in another study [9] that the particle/matrix bonding can have a significant effect on the mechanical response of the composite. Currently we are in the process of determining the wetting characteristics of the SiC particles by this alloy.

The enhanced strain-hardening behaviour of the alloy (between 10^{-3} and $2500\,s^{-1}$) is an effect of the lithium addition to the alloy, because pure aluminium and many other aluminium alloys do not exhibit a significant strain-rate effect below $10^{5}\,s^{-1}$ in the annealed condition. Lithium, being an interstitial addition in aluminium, tends to diffuse to vacancies and dislocations and can hinder the motion of dislocations. The diffusion of lithium has been shown to occur in aluminium alloys even at room temperature, and is a contributing factor to the strain-rate sensitivity of this alloy. Also, dislocation accumulation occurs more rapidly at higher strain rates. The amount of dynamic recovery occurring at higher strain rates is also smaller compared to low strain-rate testing, and is further hindered by the lithium additions. This leads

to dislocation pileups and subsequently higher strain hardening. Similar strain-rate sensitivity in 8090 alloy has also been observed under torsional loading conditions [10].

The difference in the mechanical response of the composite samples in the three directions was resolved by optical microscopy. Optical micrographs taken in the three directions revealed a significant amount of anisotropy in the particle alignment in the ED direction as compared to the TD and ND directions, Fig. 6. The particles in the ED direction are aligned as a result of the extrusion process. This alignment of the particles lends itself into producing a short-fibre composite resulting in enhanced strength. On the other hand, the particles are more uniformly distributed in the TD and ND directions. A distribution analysis for the particle aspect ratio and misorientation with respect to the extrusion axis was carried out and can be seen in Figs 7 and 8, respectively. It is evident that the aspect ratios are more spread out along the ED direction as a result of the extrusion process. On the other hand, the aspect ratios are less spread out in the ND direction. Also the misorientation angles, measured with respect to the test axis, are smaller for the particles in the ED direction as compared to the particles in the ND direction.

The differences in the orientation of the reinforcing particles with respect to the loading axis affect the deformation zones in the matrix surrounding the particles. When the sample is loaded in the ED direction, the constraint on the matrix surrounding the long side of the particles is greater than if the samples were to be loaded in the ND or TD directions (short side of the particles). The larger constraint limits the plastic deformation to the short side of the reinforcing particles, which in turn leads to a larger dislocation pileup and subsequently higher strength. On the other hand, when loaded in the ND or TD directions, the matrix in the vicinity of the long side of the particles experiences little or no constraint, thereby deforming more uniformly. This is the reason for the observed orientation effect in the composite and lack of it in the unreinforced alloy samples.

The constraint exerted by the particles on the matrix is also reflected in the thermal expansion data for the unreinforced alloy and composite samples in Fig. 9. The slope of the per cent linear change curve versus temperature (which is the coefficient of thermal expansion) is similar for the unreinforced alloy and composite samples in the ND direction, and smaller for the samples tested in the ED direction.

An equation used by Turner [11] to predict the linear coefficient of thermal expansion (CTE) of particle-reinforced composites is

$$\alpha_c = \frac{\alpha_m V_m K_m + \alpha_p V_p K_p}{V_m K_m + V_p K_p} \quad (3)$$

where α is the linear coefficient of thermal expansion, V is the volume fraction, K is the bulk modulus, and the subscripts c, m and p refer to the composite, matrix, and particle, respectively. Turner's model assumes that uniform hydrostatic stresses exist at the particle/matrix interface.

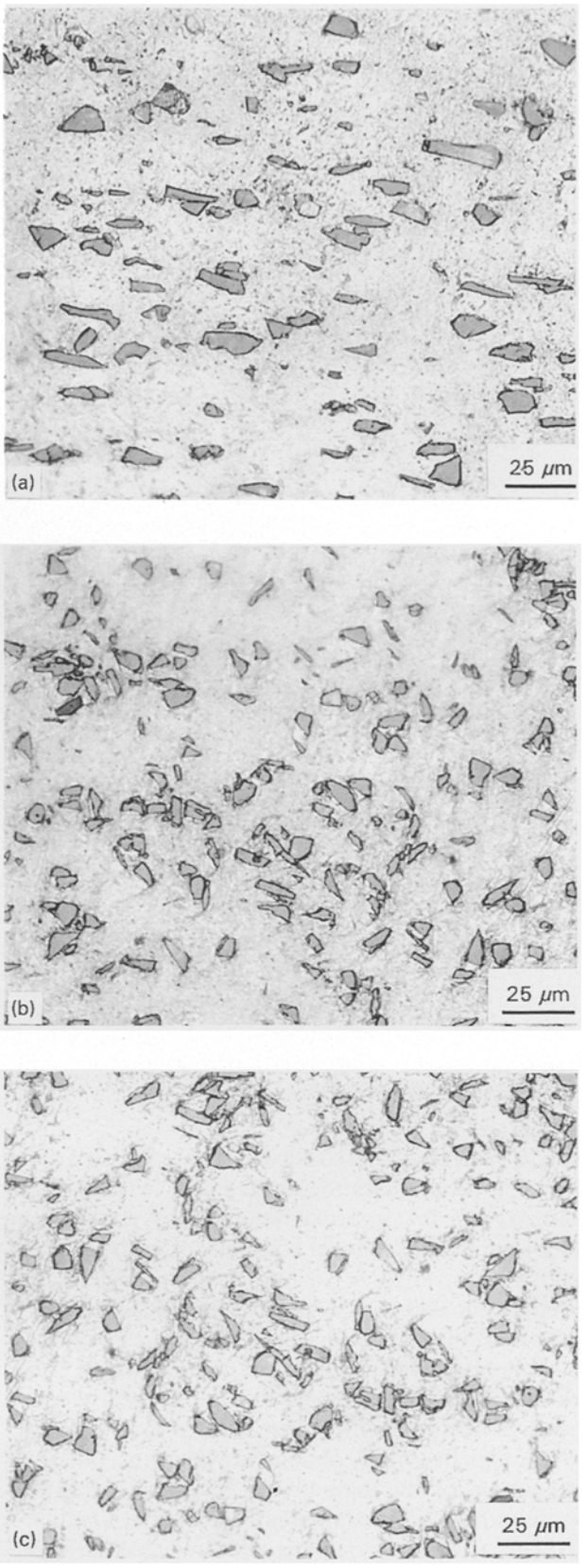

Figure 6 Optical micrographs of the composite samples illustrating the differences in the particle size and distribution. (a) ED direction, (b) TD direction, (c) ND direction.

An equation developed by Kerner [12] predicts the volumetric coefficient of thermal expansion of particle-reinforced composites as

$$\beta_c = \beta_m V_m + \beta_p V_p - (\beta_m - \beta_p) \times \frac{1/K_m - 1/K_p}{V_m/K_p + V_m/K_m + 3G_m/4} \quad (4)$$

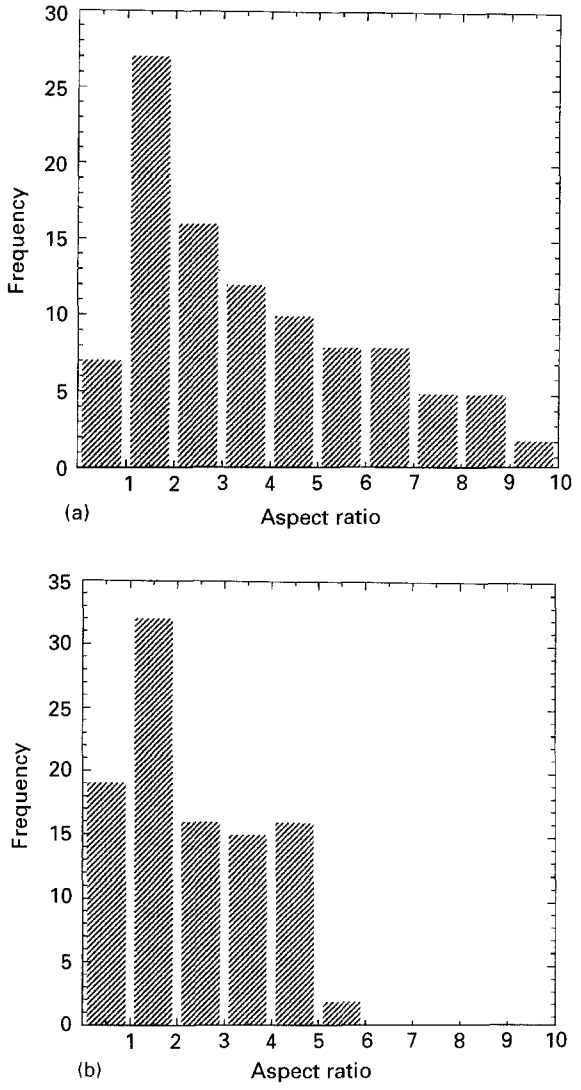

Figure 7 Distribution of the particle aspect ratio in the (a) ED direction, and (b) ND direction.

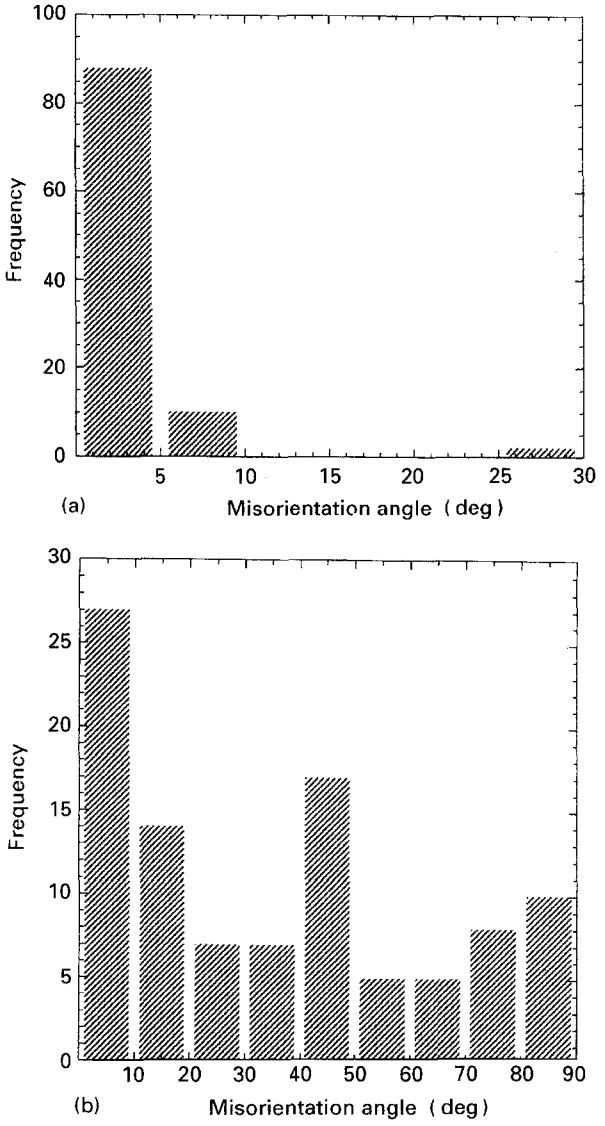

Figure 8 Distribution of the particle misorientation in the (a) ED direction, and (b) ND direction.

where β is the volume coefficient of thermal expansion (equal to three times the linear coefficient of expansion, α, as a first approximation) and G is the shear modulus. Kerner's model accounts for both the shear and isostatic stresses existing at the particle/matrix interface in such composites. Other models [13, 14] for predicting the coefficient of thermal expansion of particle-reinforced metal matrix composites are either variants of Kerner's model or have specific temperature ranges over which they can be used.

The experimentally obtained coefficients of thermal expansion for the unreinforced alloy and composite samples have been compared to the values predicted by Turner's and Kerner's models in Table III. From the results it is evident that the experimentally obtained values are in close agreement with Kerner's model. This is not unexpected, because Kerner's equation is close to a rule of mixtures approximation and the constraint term is small. This is true of particulate composites compared to fibrous composites.

Comparing the measured coefficient of thermal expansion along the ED and ND directions with the values predicted by Kerner's model, one finds that the difference between the experimental value measured along the ED direction and the value predicted by

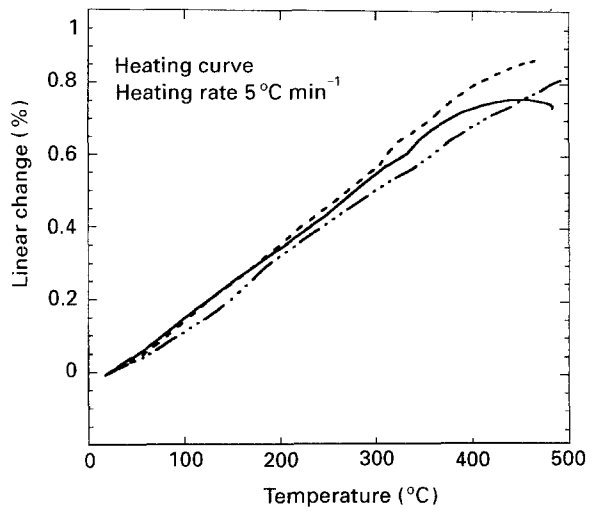

Figure 9 PLC versus temperature for (——) the unreinforced Al–Li 8090 alloy, and composite samples: (– – –) SiC_p/8090 ND direction, (— – – – —) SiC_p/8090 ED direction.

Kerner's model is very small compared to the difference between the experimental value along the ND direction and the value predicted by Kerner's model. It is important to remember that Kerner's model

TABLE III Comparison of the experimental CTE of the composite samples with the values predicted by Kerner's and Turner's models

Sample	CTE		
	Experimental ($10^{-6}\,°C^{-1}$)	Kerner's model ($10^{-6}\,°C^{-1}$)	Turner's model ($10^{-6}\,°C^{-1}$)
Al–Li 8090	21.2	–	–
SiC_p/8090: ND direction	21.4	18.4	13.9
ED direction	18.5	18.4	13.9

assumes perfect bonding and uniform distribution of the reinforcing particles. Along the ND direction, the constraint effect exerted by the particles on the matrix is small (bonding relatively weak). As a result, the expansion of the composite along the ND direction is similar to that of the unreinforced alloy. Along the ED direction, the constraint exerted by the particles on the matrix is larger (inspite of the weak bonding) because of the short-fibre effect produced as a result of the extrusion process. Hence the experimental value of the coefficient of thermal expansion along the ED direction is in closer agreement with Kerner's model as compared to the coefficient of thermal expansion measured in the ND direction.

An equation developed by Nardone and Prewo [15] predicts the enhancement in the yield strength of particle-reinforced composites, as compared to the unreinforced alloy as

$$\sigma_{cy} = \sigma_{my}[1 + (L_2 + t)S/4L_2]V_p + \sigma_{my}V_m \quad (5)$$

where σ_{cy} is the yield strength of the composite, σ_{my} is the matrix yield strength, L_2 is the length of the particle perpendicular to the applied stress, t is the particle thickness, S is the particle aspect ratio (length of the particle parallel to the applied stress divided by t), V_p is the volume fraction of the particles, and V_m is the volume fraction of the matrix.

When L_2 is much larger than t, Equation 5 reduces to

$$\sigma_{cy} = \sigma_{my}[V_p(S + 4)/4 + V_m] \quad (6)$$

Using Equation 6 we calculated a theoretical value of enhancement in the yield strength in the composite over the matrix to be 1.15 in the ED direction and 1.05 in the ND and TD directions. The experimental values, determined from the dynamic test curves, are 1.09 and 1.02, respectively. This difference again is probably because of the inadequate bonding between the SiC particles and matrix. More importantly, the ratios of the strength for a range of plastic strains of the unreinforced alloy and composite are equal, further indicating that the reinforcing particles have no effect on the strain hardening of the composite.

The ultimate strengthening observed in these composites is nowhere close to the values predicted by the rule of mixtures. Even assuming a very conservative strength value for the SiC particles, significant strengthening should be observed. However, the maximum strength of the composite is similar to that of the unreinforced alloy in the ND direction and only marginally greater along the ED direction. Also, the stiffness values determined from the low strain-rate tests are near identical for the unreinforced alloy and composite samples, further indications of a bonding problem. Studies are underway to determine the exact nature and cause of this problem.

4. Conclusion

The study has demonstrated that the strain rate has a significant effect on the mechanical response of Al–Li 8090 alloy. The strain-hardening coefficient and maximum strength (for a given strain) is significantly enhanced. This is because of the higher rate of dislocation pileup occurring at higher strain rates. Addition of SiC particles to such an alloy did not alter the mechanical behaviour of the alloy significantly. Lack of this particle influence was attributed to the weak bonding between the particles and matrix. Differences in the strength observed for the composite samples in different directions, was attributed to preferential orientation of the reinforcing particles within the composite sample as a result of the extrusion process. The thermal expansion of the alloy was not changed as a result of the SiC particles in the ND direction, because of the weak bonding. The expansion along the ED direction was altered as a result of the larger constraint exerted by the oriented particles.

Acknowledgements

The authors thank Walter Wright and Mike Lopez, Los Alamos National Laboratory, for their valuable help with the experimentation.

References

1. A. K. VASUDEVAN and R. D. DOHERTY, (eds), "Aluminum Alloys – Contemporary Research and Applications", Treatise on Materials Science and Technology, Vol. 31 (Academic Press, San Diego, 1989).
2. C. L. BUHRMASTER, D. E. CLARK and H. P. SMARTT, *J. Metals* **40** (11) (1988) 44.
3. R. H. JONES, C. A. LAVENDER and M. T. SMITH, *Scripta Metall.* **21** (1987) 1565.
4. H. J. HEINE, *Foundry Manage. Technol.* **116** (1988) 25.
5. F. A. GIROT, J. M. QUENISSET and R. NASLAIN, *Compos. Sci. Technol.* **30** (1987) 155.
6. R. U. VAIDYA, Z. R. XU, X. LI and A. K. ZUREK, *J. Mater. Sci.*, in press.

7. S. I. HONG, G. T. GRAY III and K. S. VECCHIO, *Mater. Sci. Engng*, in press.
8. S. I. HONG and G. T. GRAY III, *J. Mater. Sci.*, **29** (1994) 2987.
9. R. U. VAIDYA, S. G. SONG and A. K. ZUREK, *Philos. Mag.*, **70** (1994) 819.
10. C. Y. CHIEM, X. W. ZHOU and W. S. LEE, *J. Phys. Coll.* **C3** (1987) 577.
11. P. S. TURNER, *J. Res. NBS* **37** (1946) 239.
12. E. H. KERNER, *Proc. Phys. Soc.* **69** (1956) 808.
13. R. R. TUMMALA and A. L. FRIEDBERG, *J. Appl. Phys.* **41** (1970) 5104.
14. A. A. FAHMY and A. N. RAGAI, *ibid.* **41** (1970) 5112.
15. V. C. NARDONE and K. M. PREWO, *Scripta Metall.* **20** (1986) 797.

Received 15 June
and accepted 16 September 1994